Eidgenössische Technische Hochschule Zürich
Swiss Federal Institute of Technology Zurich

PAUL SCHERRER INSTITUT

Semester Thesis

Design study for Laser Plasma Wakefield Acceleration of low Energy Electrons

Nick Sauerwein

supervised by
Dr. Andreas Adelmann

September 19, 2016

Abstract

This paper presents a derivation of a simple linear model of plasma wake field acceleration. The model is then used to design an experiment which will be performed at the Paul-Scherer-Institut in Switzerland. The basic ideas are to first explain how plasma acceleration works and show that it is possible to construct such an accelerator in the scope of a master thesis. Later the experiment may be used for other physics students to get familiar with the concept of Plasma Wake Field Acceleration.

Contents

1 Introduction

Laser Wake Field Acceleration (LWFA) is a method to accelerate electrons to very high energies within short distances. The electric field involved in such a device are by factors up to 1000 higher then in conventional accelerators. The idea is to shoot an extremely energetic (mJ to J) shortly pulsed laser trough a plasma, which might be self generated (ionization) or generated by a discharge. The ponderomotive force of the laser then generates a region of lower electron density in the plasma. Since the nuclei are much heavier than electrons they remain almost stationary. Therefore the laser creates a charge separation and so a strong electric field is generated. The charge density wave will propagate behind the laser. By so called injection methods one can achieve that some electrons become trapped in the wake and get accelerated to a few MeV within a millimeter. One should think of a surfer on a wake of a boat in this case, where the boat represents the laser, the surfer the accelerated electron bunch and the ocean the plasma electrons which generate the wake.

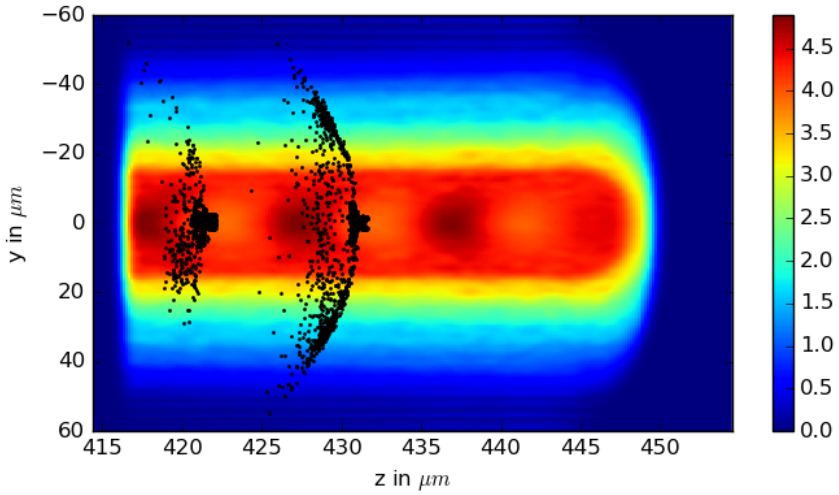

Figure 1: 2D electron density profile in arbitrary units when laser travels through plasma. The black dots represent strongly accelerated electrons. This plot was done using a PIC simulation presented in Section 5.2.

This write-up is split into three major parts. First the analytic linear model is derived and discussed in detail (Section 3). Second a short introduction into injection methods is given, however the focus is put on density down-ramp injection (4). Furthermore the solutions to the acceleration problem are integrated numerically with two different approaches. First the trajectory of a single electron in the wakefield obtained by the linear model (Section 5.1) is studied and second a full simulation of the process using the Particle-in-Cell (PIC) code WARP (Section 5.2) is discussed. This steps are necessary to design an experiment setup for LWFA as it will be done at PSI.

2 Constraints of the Design

Since the goal of this paper is to present how to design a low energy laser wake field accelerator. We first have to discuss the constraints that we are facing in the setup. First of all it is to mention that this project is performed by students, so financial resources are rather low. The setup have to fully rely on equipment that is already present at PSI.

The major cost of a LWFA is the laser itself. PSI owns a 40 mJ pulsed Ti-Sa laser of 800 nm wavelength, which can generate pulses of duration of about 15 fs and a focal waist of around 10 µm. This laser has, as shown throughout the paper, satisfies perfect conditions for a low energy LWFA.

Another goal is to use the most simplistic setup of the experiment. We want to show that with the current knowledge about LWFA it is possible to design and construct a accelerator within less than two years from scratch.

3 Model for Plasma Wake Field Acceleration

In this section a linear model for plasma wake field acceleration is derived. It follow the ideas found in the papers ([7], [8]). In order to solve the equations some assumptions have to be made. In the section 3.9 it is discussed in detail why it is legitimate to use them and what is the order of error error that is done. The derivation follows the following path. The first step is to describe the plasma as an relativistic charged Euler fluid, which can interact with a electromagnetic field through the Lorenz force. This results in a set of partial differential equations, which can be brought in an dimensionless form. The most important parameter of laser plasma interaction is the dimensionless vector potential

$$\vec{a} = \frac{\vec{A}e}{mc^2}.$$

For the calculation the assumption that $\vec{a} \ll 1$ is taken, so that the equations can be expanded to second order in $\vec{a}$ in order to remain with a linear inhomogeneous partial differential equation. These equations can be solved using the greens function. For an assumed shape of the incoming laser pulse (inhomogeneous part) a analytically solution to the plasma waves induced by the pulse is integrated. With conservation of energy the depletion of the laser is externally put into the model and the wave equation in the paraxial approximation describes the motions of the laser pulse in the plasma (defocussing).

3.1 Plasma Equations

Since the nuclei are assumed to be at rest, the plasma is described as an infinitely extended charged electron gas which a positive homogeneous background charge. The interaction withing the gas takes place via the Coulomb force. The boundary (point where laser enters the plasma) are set to be at $z = 0$ and the laser pulse propagates initially along z-direction. The dynamics of the electric and magnetic fields are given by the Maxwell equations. Which will write down in a from only using the vector potential $\vec{A}$ and the electrostatic potential ϕ. Also throughout the calculations coulomb gauge will be used.

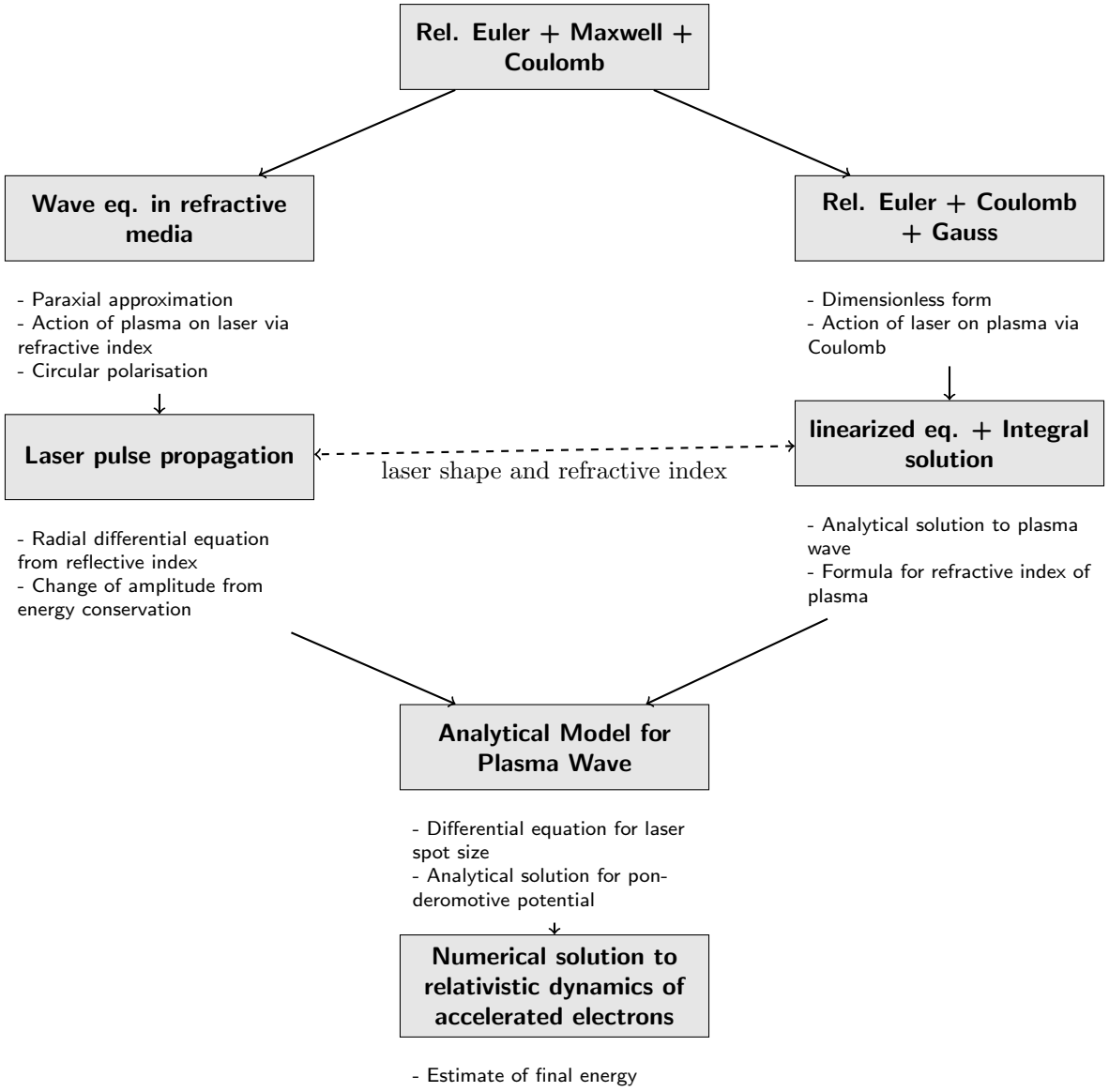

Figure 2: Schematic overview of calculation

The set of equations have the form ([3],[8]):

$$\frac{D}{Dt}(\gamma m\vec{v}) = e\left(\vec{\nabla}\Phi + \frac{1}{c}\frac{\partial\vec{A}}{\partial t} - \frac{\vec{v}}{c}\times(\vec{\nabla}\times\vec{A})\right) \quad \text{Momentum conservation} \quad (3.1.1)$$

$$\frac{\partial n}{\partial t} + \vec{\nabla}\cdot(n\vec{v}) = 0 \quad \text{Continuity equation} \quad (3.1.2)$$

$$\vec{\nabla}\cdot\vec{A} = 0 \quad \text{Coulomb gauge} \quad (3.1.3)$$

$$\Delta\Phi = 4\pi e(n - n^0) \quad \text{Gauss} \quad (3.1.4)$$

$$\Delta\vec{A} - \frac{1}{c^2}\frac{\partial^2\vec{A}}{\partial t^2} = \frac{4\pi}{c}ne\vec{v} + \frac{1}{c}\vec{\nabla}\frac{\partial\Phi}{\partial t} \quad \text{Inhomogenious wave equation} \quad (3.1.5)$$

where n^0 is the background ion density and $\gamma = \frac{1}{\sqrt{1-(\frac{v}{c})^2}}$ is the relativistic factor. Note that $\frac{D}{Dt} = \frac{\partial}{\partial t} + (\vec{v} \cdot \vec{\nabla})$ is the generalized time derivative for fluids in motion.

3.2 Simplification of Plasma Equations

In this section we want to derive a more illustrative form for the plasma equation, which is dimensionless and can be linearized easily. Starting by bringing the momentum equation 3.1.1 in its canonical from, we define

$$\vec{P} = \gamma m \vec{v} - \frac{e}{c}\vec{A} \tag{3.2.1}$$

as the canonical momentum of an electron in a field $\vec{A}$. Equation 3.1.1 is then rewritten as

$$\frac{\partial \vec{P}}{\partial t} = \vec{\nabla}(e\Phi - \gamma m c^2) + \vec{v} \times (\vec{\nabla} \times \vec{P}) \tag{3.2.2}$$

where the definition of $\vec{P}$, the coulomb gauge and the fact that $\vec{v} \times (\vec{\nabla} \times \vec{v}) = 0$ have been used. Using the fact that we can write the momentum $\vec{P} = \alpha\vec{\nabla}\beta + \vec{\nabla}\Psi$, where α, β and Ψ are scalar functions of space and time the momentum equation 3.2.2 can be further modified to

$$\vec{\nabla}\left(\frac{\partial \Psi}{\partial t} - e\Phi + \gamma m c^2 + \alpha\frac{\partial \beta}{\partial t}\right) = \left(\frac{\partial \beta}{\partial t} + \vec{v} \cdot \vec{\nabla}\beta\right)\vec{\nabla}\alpha - \left(\frac{\partial \alpha}{\partial t} + \vec{v} \cdot \vec{\nabla}\alpha\right)\vec{\nabla}\beta$$

which can be separated to a set of three independent equations

$$\begin{aligned}
&\frac{\partial \Psi}{\partial t} - e\Phi + \gamma m c^2 + \alpha\frac{\partial \beta}{\partial t} = -C_0(t) \\
&\frac{\partial \beta}{\partial t} + \vec{v} \cdot \vec{\nabla}\beta = 0 \\
&\frac{\partial \alpha}{\partial t} + \vec{v} \cdot \vec{\nabla}\alpha = 0.
\end{aligned}$$

$C_0(t)$ is the integration constant which comes from solving the equation of type $\vec{\nabla}(...) = 0$. Seliger and Whitham ([14], [6]) showed that we can write all the plasma describing equations in a variational principle of the form

$$\begin{aligned}
\delta \int_{t_1}^{t_2} \int \Bigg\{ &\frac{1}{8\pi}\left[(\vec{\nabla} \times \vec{A})^2 - \left(\vec{\nabla}\Phi + \frac{1}{c}\frac{\partial \vec{A}}{\partial t}\right)^2\right] \\
&+ n\left(\frac{\partial \Phi}{\partial t} + \alpha\frac{\partial \beta}{\partial t} + \gamma m c^2 - e\Phi - C_0(t)\right) + n^0 e\Phi \Bigg\} d\vec{r}dt = 0.
\end{aligned} \tag{3.2.3}$$

Since in the region ahead of the laser pulse the plasma is still in thermal equilibrium, which is approximated as totally at rest ($\gamma = 1, \frac{\partial \Psi}{\partial t} = \alpha = \beta = \Phi = 0$), we find

$$C_0(t) = mc^2$$

as an value for the integration constant. Taking the curl of the canonical momentum equation (3.2.2) yields

$$\frac{\partial}{\partial t}\left(\vec{\nabla}\times\vec{P}\right)=\vec{\nabla}\times\left(\vec{v}\times\left(\vec{\nabla}\times\vec{P}\right)\right)$$

This equation stats, that if $\vec{\nabla}\times\vec{P}=0$ initially, which is the case for the plasma without the laser, it will remain zero for all time. Therefore $\vec{P}$ can be expressed only by a scalar function Ψ and $\alpha=\beta=0$ can be set zero. To make the equations dimensionless we rescale the variables by

$$\Phi\to\frac{mc^2}{e}\Phi,\ \vec{A}\to\frac{mc^2}{e}\vec{a},\ n\to n\bar{n},\ n^0\to n^0\bar{n},\ t\to\frac{t}{\omega_L},\ \vec{r}\to\frac{\vec{r}}{k},\ \Psi\to\frac{mc^2\Psi}{\omega_0}. \quad (3.2.4)$$

The transformed variational equation 3.2.3 reads

$$\left(\frac{m^2c^4k}{4\pi e^2\omega}\right)\delta\int_{t_1}^{t_2}\int\left\{\frac{1}{2}\left[(\vec{\nabla}\times\vec{a})^2-\left(\vec{\nabla}\Phi+\frac{\partial\vec{a}}{\partial t}\right)^2\right]\right.$$
$$\left.+\epsilon^2n\left(\frac{\partial\Phi}{\partial t}+\gamma-\Phi-1\right)+\epsilon^2n^0e\Phi\right\}d\vec{r}dt=0$$

where $\epsilon=\omega_p/\omega_L$, $\gamma=\sqrt{1+(a+\vec{\nabla}\Psi)^2}$ and ω_L is the frequency of the laser. The plasma frequency

$$\omega_p=\sqrt{4\pi\bar{n}e^2/m} \quad (3.2.5)$$

is here the defining physical quantity of the plasma. ω_L has been chosen to make the time dimensionless to make all equations dependent only depend on ϵ. The Euler-Lagrange equations now yield the dimensionless set of plasma equations

$$\frac{\partial\Psi}{\partial t}+\gamma-\Phi-1=0 \quad (3.2.6)$$
$$\frac{\partial n}{\partial t}+\vec{\nabla}\cdot\left(\frac{n}{\gamma}\vec{\nabla}\Psi\right)+\vec{\nabla}\frac{n}{\gamma}\cdot\vec{a}=\frac{\partial n}{\partial t}+\vec{\nabla}\cdot\frac{n}{\gamma}\left(\vec{\nabla}\Psi+\vec{a}\right)=0 \quad (3.2.7)$$
$$\Delta\Phi=\epsilon^2(n-n^0) \quad (3.2.8)$$
$$\Delta\vec{a}-\frac{\partial^2\vec{a}}{\partial t^2}=\epsilon^2\frac{n}{\gamma}(\vec{a}+\vec{\nabla}\Psi)+\vec{\nabla}\frac{\partial\Phi}{\partial t}. \quad (3.2.9)$$

In addition to the above equations we still have the coulomb gauge

$$\vec{\nabla}\cdot\vec{a}=0. \quad (3.2.10)$$

Taking the gradient of equation 3.2.6 and using the relation $\vec{P}=\vec{\nabla}\Psi$, one obtains

$$\vec{\nabla}\Psi=(\gamma\vec{\beta}-\vec{a})=\delta\vec{u} \quad (3.2.11)$$

as an dimensionless version of 3.2.1, where $\vec{u}=\vec{\beta}\gamma$ and $\delta\vec{u}=\vec{u}-\vec{a}$ represent the dimensionless velocity and canonical momentum. Equation 3.2.6 can now be rewitten as

$$\frac{\partial\delta\vec{u}}{\partial t}=\vec{\nabla}(\Phi-\gamma). \quad (3.2.12)$$

This equation fully describes the action of the laser on the plasma. The first term is the space charge force and the second the generalized ponderomotive force $F_p=-mc^2\vec{\nabla}\gamma$.

3.3 Plasma Waves in the Linear Regime

The reset of the derivation is based on the expansion of each quantity in powers of a, i.e. every quantity Q is expressed as $Q = \sum Q_n$ where $Q_n \propto a^n$. The linear approximation is to truncate this series after the second order in a. The zeroth order describes the plasma in absence of a laser pulse, $n_0 = n^0 \overset{dimless}{=} 1$, $\gamma_0 = 1$, $\vec{u}_0 = 0$. Note that from now on n_0 are identical n^0 since the zeroth order in n corresponds to the background density n^0. This is due to the fact that a neutral plasma is studied. The first order corresponds to the quiver motion (compare to the derivation in section 4.1), i.e. $\vec{u}_1 = \vec{a}_1 = \vec{\beta}_1$ and $n_1 = \gamma_1 = \Phi_1 = 0$. The second order is contained by the modified momentum equation 3.2.12

$$\frac{\partial \vec{u}_2}{\partial t} = \vec{\nabla}(\Phi_2 - a^2/2). \tag{3.3.1}$$

Here $\gamma = \sqrt{1+p^2} \approx \sqrt{1+a^2} \approx 1 + a^2/2$ has been used. For the continuity 3.2.7 and Poisson equation 3.2.8

$$\Delta\Phi_2 = \epsilon^2 n_2 \tag{3.3.2}$$

$$\frac{\partial n_2}{\partial t} + \vec{\nabla}(n_0 \vec{\beta}_2) = 0 \tag{3.3.3}$$

can be derived as equations for the second order expansion. Inserting the equations in each other finally yields

$$\left(\frac{\partial^2}{\partial t^2} + \epsilon^2\right) \Phi_2 = \epsilon^2 \frac{a^2}{2}$$
$$\left(\frac{\partial^2}{\partial t^2} + \epsilon^2\right) \frac{n_2}{n_0} = \Delta \frac{a^2}{2}$$
$$\left(\frac{\partial^2}{\partial t^2} + \epsilon^2\right) \vec{\beta}_2 = -\frac{\partial}{\partial t} \vec{\nabla} \frac{a^2}{2}$$

which is a set of three decoupled inhomogeneous harmonic oscillators with frequency $\epsilon = \omega_p/\omega$. Using the Greens function $G(t,t') = \Theta(t-t')\frac{1}{\epsilon}\sin(\epsilon(t-t'))$ we can integrate the equations to

$$\Phi_2 = \epsilon \int_0^t \sin(\epsilon(t-t')) \frac{a^2}{2} dt' \tag{3.3.4}$$
$$\frac{n_2}{n_0} = \frac{1}{\epsilon} \int_0^t \sin(\epsilon(t-t')) \Delta \frac{a^2}{2} dt'$$
$$\vec{\beta}_2 = -\frac{1}{\epsilon} \int_0^t \sin(\epsilon(t-t')) \frac{\partial}{\partial t'} \vec{\nabla} \frac{a^2}{2} dt'.$$

Since all the integrals are connected through the equations 3.3.1, 3.3.2 and 3.3.3, it is enough to solve the integral for $\Phi = \Phi_2$. A solution for a sinus laser pulse shape is given in section 3.5.1.

3.4 Refractive Index in a Plasma

Analysing the wave equation 3.2.9

$$\left(\Delta - \frac{\partial^2}{\partial t^2}\right)\vec{a} = \epsilon^2 \frac{n}{\gamma}(\vec{a} + \vec{\nabla}\Psi) + \vec{\nabla}\frac{\partial \Phi}{\partial t} \overset{3.2.11}{=} \epsilon^2 n\vec{\beta} + \vec{\nabla}\frac{\partial \Phi}{\partial t}.$$

the refective index of electromagetic waves in a plasma can be found. Since the laser fields are purely rotational, terms like $\vec{\nabla}\frac{\partial \Phi}{\partial t}$ can be neglected to get

$$\left(\Delta - \frac{\partial^2}{\partial t^2}\right)\vec{a} = \epsilon^2 n\vec{\beta}. \tag{3.4.1}$$

The next step is to use the Poisson equation 3.2.8, to show that in first order of $\vec{a}$, n is constant

$$\Delta\Phi = \epsilon^2(n - n^0) \overset{3.2.6}{=} \Delta\gamma. \tag{3.4.2}$$

which yields

$$n = n_0 + \frac{1}{\epsilon^2}\Delta\gamma. \tag{3.4.3}$$

Since $\Delta\gamma$ is at least second order in a, equation3.4.1 can be solved by setting $n \approx n_0$ and $\vec{u} = \vec{a}$, and so

$$\left(\Delta - \frac{\partial^2}{\partial t^2}\right)\vec{a} = \epsilon^2 n_0 \frac{\vec{a}}{\gamma}. \tag{3.4.4}$$

A good Ansatz for the vector potential of a laser pulse traveling is

$$\vec{a} = \Re\left[a\ \ \vec{\sigma}\exp[i(kz - \omega t)]\right].$$

Then 3.4.4 becomes

$$\omega^2 = k^2 + \epsilon^2 n_0/\gamma.$$

as the dispersion relation. The refractive index is then calculated bz

$$\begin{aligned}
\eta_r &= \frac{d\omega}{dk} \\
&= \sqrt{1 - \frac{\epsilon^2 n_0}{\omega^2 \gamma}} \\
&= \sqrt{1 - \frac{\epsilon^2 n_0}{\omega^2\sqrt{1 + a^2}}} \\
&\approx 1 - \frac{\epsilon^2 n_0}{2\omega^2}.
\end{aligned} \tag{3.4.5}$$

Because ω_L was used to make the time dimensionless in the transformation 3.2.4, the laser corresponds to $\omega = 1$.

3.5 Propagation of Laser Pulses in Reflective Media

This derivation follows directly the ideas of [8]. In order to describe a laser pulse in refractive media the wave equation of the form

$$\left(\vec{\nabla}^2 - \frac{\partial^2}{\partial t^2}\right)\vec{a} = (1-\eta_r^2)\ \vec{a} \tag{3.5.1}$$

has to be solved. Here $\vec{a}$ is the dimensionless vector potential of the laser and η_r the refractive index of the material. The equation corresponds directly to 3.4.1. For a plasma η_r is derived in section 3.4. In vacuum $\eta_r = 1$ and the equation reduces to the homogeneous wave equation. It is important that for the further analysis cylindrical symmetry is assumed. This means means $\vec{a} = \vec{a}(r, z, \xi)$ and $\vec{\nabla}^2 = \vec{\nabla}_\perp^2 + \frac{\partial^2}{\partial z^2}$, where $\xi = z - \beta_g t$ is the co moving coordinate and β_g is the dimensionless group velocity of the pulse ($\beta_g \approx 1$).

We will assume that we can write

$$\vec{a} = \mathrm{Re}\ \ \vec{a}_0 g(r,z) f(\xi) \exp[i\xi] \tag{3.5.2}$$

g and f are the slowly varying envelope of the pulse, i.e.

$$\left|\frac{\partial f, g}{\partial t}\right| \ll |f, g| \ \text{ and } \ \left|\frac{\partial f, g}{\partial z}\right| \ll |f, g|\,.$$

$f(\xi)$ is the longitudinal shape of the pulse and $g(r, z)$ the traversal. The paraxial approximation which claims that $\left|\frac{\partial a}{\partial \xi}\right| \ll \left|\frac{\partial a}{\partial z}\right|$. Because the wave equation is linear we can drop the Re for the next calculation. Substituting the Ansatz 3.5.2 into the wave equation yields

$$\left(\vec{\nabla}^2 - \frac{\partial^2}{\partial t^2}\right)\vec{a} \approx$$

$$\vec{\nabla}_\perp^2 \vec{a} + 2i\left(2\frac{\partial f}{\partial \xi} g + f\frac{\partial g}{\partial z}\right)\vec{a}_0 \exp[i\xi] \approx \vec{\nabla}_\perp^2 \vec{a} + 2if\frac{\partial g}{\partial z}\vec{a}_0 \exp[i\xi]$$

$$= (1-\eta_r^2)\vec{a}$$

,which can be written as

$$\left(\vec{\nabla}_\perp^2 + 2i\frac{\partial}{\partial z}\right) g = (1-\eta_r^2)\ \ g. \tag{3.5.3}$$

This equation is solved with the Ansatz that g is of the form

$$g(r,z) = g_0(z) r_0/r_s \exp[-(1-i\alpha_s)r^2/r_s^2 + i\theta_s],$$

where r_0 is a constant, $r_s(z)$ is the spot size. $\theta_s(z)$, $\alpha_s(z)$ and $g_0(z)$ are real functions. Note that the power P of the wave is only dependent on z through $g_0(z)$

$$\begin{aligned} P &\propto \int dr r\,|g|^2 \\ &= \int dr r g_0^2 r_0^2/r_s^2 \exp[-2r^2/r_s^2] \\ &= \frac{1}{4} g_0^2 r_0^2. \end{aligned}$$

The following calculation will be very painful, but it has a very simple result. The idea is to plug the Gaussian Ansatz in the paraxial wave equation and then find a differential equation for the spot size $r_s(z)$. In particular the paraxial wave equation is evaluated and then separate it in powers of r and real and imaginary part. The refractive index is

$$\begin{aligned}\eta_r &= \sqrt{1 - \frac{\epsilon^2 n_0}{\omega^2\sqrt{1+a^2}}} \\ &\approx \sqrt{1 - \frac{\epsilon^2 n_0}{\omega^2}(1 - a^2/2)}\end{aligned}$$

as derived in section 3.4, where we will expand the radial dependence of a^2 in powers of r, i.e. $a^2 \propto \exp(-2r^2/r_s^2) \approx (1 - 2r^2/r_s^2)$. In the middle of the lengthy calculation the paraxial wave equation reduces to

$$\begin{aligned}r^2\left[\frac{4}{r_s^2}(1-\alpha_s^2) + \frac{4}{r_s^3}\frac{\partial r_s}{\partial z}\alpha_s - \frac{2}{r_s^2}\frac{\partial \alpha_s}{\partial z}\right] + \left[-\frac{4}{r_s^2} - 2\frac{\partial \theta_s}{\partial z}\right] + i\left[r^2\left[-2\alpha_s\frac{4}{r_s^4} + \frac{4}{r_s^3}\frac{\partial r_s}{\partial z}\right]\right. \\ \left. + \left[\frac{4}{r_s^2}\alpha_s + 2\frac{\partial g_0}{\partial z}/g_0 - 2\frac{\partial r_s}{\partial z}/r_s\right]\right] = r^2\epsilon^2 n_0 a_0^2 g_0^2 \frac{r_0^2}{r_s^2} + \left[\epsilon^2 n_0(1 - \frac{r_0^2 a_0^2 g_0^2}{2r_s^2})\right].\end{aligned}$$

Assuming $\left|\frac{\partial r_s}{\partial z}/r_s\right| \gg \left|\frac{\partial g_0}{\partial z}/g_0\right|$ the Ansatz 3.5 reduced the wave equation 3.5.3 to

$$\begin{aligned}\frac{\partial \theta_s}{\partial z} &= -\frac{2}{r_s^2} + \frac{\epsilon^2 n_0}{2}(\frac{r_0^2 a_0^2 g_0^2}{2r_s^2}) \\ \alpha_s &= \frac{r_s}{2}\frac{\partial r_s}{\partial z} \\ \frac{\partial^2 r_s}{\partial z^2} &= \frac{1}{r_s^3}\left[4 - \epsilon^2 n_0 a_0^2 g_0^2\right].\end{aligned} \tag{3.5.4}$$

θ_s and α_s are of no further interest calculations they will just shift the phase of our wave and the generated wave in linear approximation only depends on the second order in a. Now the problem of defocusing in a plasma reduces to integrating the ODE 3.5.4 for a given $g_0(z)$.

3.5.1 Solution to Plasma Equations in the Linear Regime

For the following discussion the shape of our incoming laser pulse is fixed. The shape of a is chosen such that equation 3.3.4 becomes analytically solvable. The envelope $a = |\vec{a}|$ of the pulse is thought to have the form

$$a = a_0 f(\xi) g(r, z)$$

where $\xi = z - \beta_g t$ and

$$\begin{aligned}f(\xi) &= \begin{cases}\sin(\frac{\pi}{L}\xi), & \text{if } 0 < \xi < L \\ 0, & \text{elsewhere}\end{cases} \\ g(r) &= g_0(z)\frac{r_0^2}{r_s(z)^2} exp(-r^2/r_s(z)^2)\end{aligned}$$

Then the electrostatic potential ϕ can be written as the integral (3.3.4)

$$\Phi = \Phi_2 = \Phi^0(r,z)\ \epsilon \int \sin(\epsilon(t-t'))\sin^2(\frac{\pi}{L}\xi)dt',$$

where $\Phi^0(r) = \frac{1}{2}a_0^2 g^2(r,z)$. Length of the pulse L must be chosen such that the magnitude of the electric potential Φ is maximal. This is the case if $L \approx \lambda_p$, so will choose

$$L = \frac{2\pi\beta_g}{\epsilon} \tag{3.5.5}$$

for our calculation.

$$\begin{aligned}\Phi &= \Phi^0(r,z)\epsilon \int \sin(\epsilon(t-t'))\sin^2(\frac{\epsilon}{2\beta_g}\xi)dt' \\ &= \Phi^0(r,z)\frac{1}{16}\left[-2\epsilon t'\sin(\epsilon t - \epsilon/\beta_g z) - \cos(\epsilon t - 2\epsilon t' + \epsilon/\beta_g z) + 4\cos(\epsilon(t-t'))\right]\end{aligned}$$

In the next step we need to set the boundaries conditions. After that we can decompose the plasma wake in three different parts. Part Tail (T) is the part where the pulse enters the plasma, Part Wave (W) is the harmonic part of the plasma wave and Part Front (F) is the laser spot.

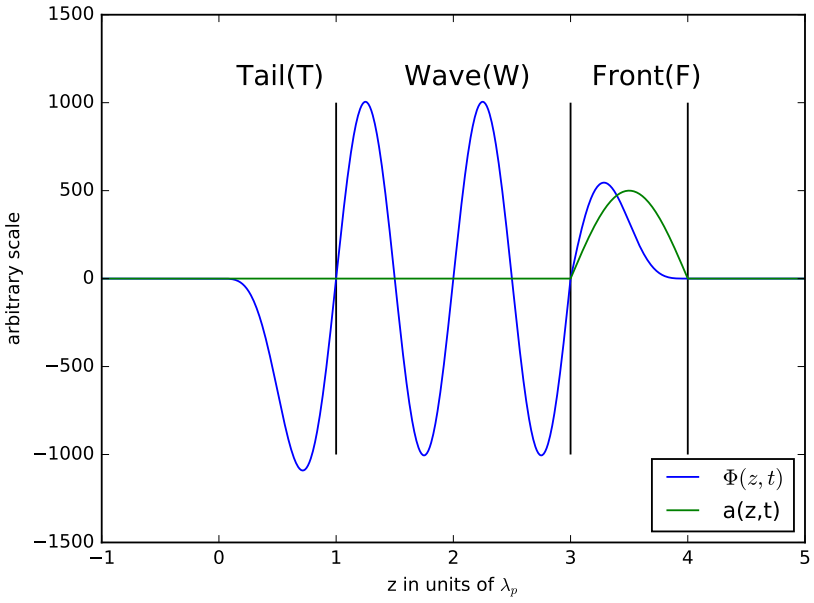

Figure 3: Plot of the analytical solution of the plasma wave Φ for $r = 0$. The plasma begins at $z = 0$ and extends to infinity. The acceleration of the electrons will take place in the part W of the wave.

For these parts we find the following solutions:

$$\begin{aligned}
\Phi_T(r,z,t) &= \Phi^0(r,z)\frac{1}{8}\left[2\frac{\epsilon}{\beta_g}z\sin(k_p\xi) + 3\cos(\frac{\epsilon}{\beta_g}\xi) + \cos(\epsilon(t+\frac{1}{\beta_g}z)) - 4\cos(\epsilon t)\right] \\
\Phi_W(r,z,t) &= \Phi^0(r,z)\frac{\pi}{2}\sin(\frac{\epsilon}{\beta_g}\xi) \\
\Phi_F(r,z,t) &= \Phi^0(r,z)\frac{1}{8}\left[(2\pi - \frac{\epsilon}{\beta_g}\xi)\sin(\frac{\epsilon}{\beta_g}\xi) + 8\sin^2(\frac{\epsilon}{2\beta_g}\xi)\right]
\end{aligned} \tag{3.5.6}$$

3.6 Depletion of a Laser Pulse Due to Plasma Wave Generation

In order to estimate how the laser pulse amplitude a_0 depletes with respect to the propagation distance z energy conservation is applied. By assumption the energy contained in the electromagnetic field of the laser will only be used to create the plasma wave, i.e. thermal effects, collisions and the energy going into the acceleration of the particle bunch are neglected. In equations that means that

$$\frac{\overline{\partial U_p}}{\partial z} = -\frac{\partial U_L}{\partial z}, \tag{3.6.1}$$

where U_L is equal to the energy stored in the laser pulse and $\overline{U_p}$ to the energy stored in the plasma wave averaged over one plasma wavelength. Clearly the averaging is an approximation, but this makes the final equations much simpler. $\lambda_p \ll L_{dp}$ legitimizes that approximation. For the following discussion the energies stored in the front (F) and tail (T) parts of the plasma wave are neglected. The energy density of an electromagnetic field is given by

$$u_{em} = \frac{1}{8\pi}\left(E^2 + B^2\right).$$

$\frac{\partial U_p}{\partial z}$ can be integrated to

$$\begin{aligned}
\frac{\partial U_p}{\partial z} &= \int u_{em} r dr d\phi = 2\pi \int u_{em} r dr \\
&= \frac{1}{4}\int E_p^2 r dr
\end{aligned}$$

where E_p is the electrostatic field of the plasma wave and the magnetic field generated by the moving electrons since that is proportional to β and therefore higher order in a. E_p is given by the modulus of the negative gradient applied on the potential given by equation 3.5.6.

$$\begin{aligned}
\vec{E_p} = -\vec{\nabla}\Phi &= -\frac{\pi}{4}a_0^2\vec{\nabla}\left(g^2(r,z)\sin(\frac{\epsilon}{\beta_g}\xi)\right) \\
&= -\frac{\pi}{4}a_0^2 g^2(r,z)\begin{pmatrix} -4\frac{r}{r_s(z)^2}\sin(\frac{\epsilon}{\beta_g}\xi) \\ \frac{\epsilon}{\beta_g}\cos(\frac{\epsilon}{\beta_g}\xi) + 2\left(\frac{\partial g_0}{\partial z}/g_0 - (1-\frac{r^2}{r_s^2})\frac{\partial r_s}{\partial z}/r_s\right)\sin(\frac{\epsilon}{\beta_g}\xi)\end{pmatrix} \\
&= \begin{pmatrix} -4\frac{r}{r_s(z)^2}\sin(\frac{\epsilon}{\beta_g}\xi) \\ \frac{\epsilon}{\beta_g}\cos(\frac{\epsilon}{\beta_g}\xi)\end{pmatrix}.
\end{aligned}$$

The second term was neglected because the plasma wavelength is much smaller than the length of depletion $\lambda_p \ll L_{dp}$. In this approximation E_p^2 is given by

$$E_p^2 = \frac{\pi^2}{16} a_0^4 g^4(r,z) \left[16 \frac{r^2}{r_s^4} \sin^2(\frac{\epsilon}{\beta_g}\xi) + \frac{\epsilon^2}{\beta_g^2} \cos^2(\frac{\epsilon}{\beta_g}\xi) \right].$$

Integrating this function over the radius gives

$$\begin{aligned}
\frac{\partial U_p}{\partial z} &= \frac{\pi^2}{32} a_0^4 \int g^4(r,z) \left[16 \frac{r^2}{r_s^4} \sin^2(\frac{\epsilon}{\beta_g}\xi) + \frac{\epsilon^2}{\beta_g^2} \cos^2(\frac{\epsilon}{\beta_g}\xi) \right] r dr \\
&= \frac{\pi^2}{32} a_0^4 g_0^4 \frac{r_0^4}{r_s^4} \left[\frac{16}{r_s^4} \sin^2(\frac{\epsilon}{\beta_g}\xi) \underbrace{\int r^3 \exp(-4r^2/r_s^2) dr}_{3/16 r_s^4} + \frac{\epsilon^2}{\beta_g^2} \cos^2(\frac{\epsilon}{\beta_g}\xi) \underbrace{\int r \exp(-4r^2/r_s^2) dr}_{r_s^2/4} \right] \\
&= \frac{\pi^2}{32} a_0^4 g_0^4 \frac{r_0^4}{r_s^4} \left[3 \sin^2(\frac{\epsilon}{\beta_g}\xi) + \frac{1}{4} \frac{\epsilon^2}{\beta_g^2} r_s^2 \cos^2(\frac{\epsilon}{\beta_g}\xi) \right].
\end{aligned}$$

Averaging over one plasma wavelength λ_p yields

$$\overline{\frac{\partial U_p}{\partial z}} = \frac{\pi^2}{64} a_0^4 g_0^4 \frac{r_0^4}{r_s^4} \left[3 + \frac{1}{4} \frac{\epsilon^2}{\beta_g^2} r_s^2 \right].$$

In the next step of the calculation the energy stored in the laser pulse is computed for a fixed $g(z)$. Here we say that g(z) is constant over the extension of the laser pulse.

$$\begin{aligned}
u_{em} &= \frac{1}{8\pi} \left(E_L^2 + B_L^2 \right) \\
&= \frac{1}{8\pi} \left(\left(\frac{\partial \vec{a}}{\partial t} \right)^2 + \left(\vec{\nabla} \times \vec{a} \right)^2 \right) \\
&= \frac{1}{4\pi} a^2 \\
&= \frac{1}{4\pi} a_0^2 f^2(\xi) g^2(r,z)
\end{aligned}$$

which can be integrated to

$$U_L = \frac{1}{16} a_0^2 r_0^2 g_0^2(z) L.$$

Using the energy conservation 3.6.1 finally gives

$$\frac{\partial g_0}{\partial z} = -\frac{\pi}{4} a_0^2 \frac{r_0^2}{r_s^2} g_0^3 \frac{\epsilon}{\beta_g} \left(\frac{3}{r_s^2} + \frac{1}{4} \frac{\epsilon^2}{\beta_g^2} \right). \tag{3.6.2}$$

3.7 Acceleration of Electrons in Linear Plasma Wake Fields

In order to describe the motion of an electron in the wake field, the result for the electrostatic potential of the plasma wave 3.5.6 is used. The equation of motion in the laboratory

frame can than be written as [4]

$$\begin{aligned}\frac{\partial \vec{u}}{\partial t} &= \frac{\partial \gamma \vec{\beta}}{\partial t} \\ &= -\vec{E} \\ &= \vec{\nabla}\Phi_W(r,z,t).\end{aligned}$$

Under the assumption that only the longitudinal motion of the electron is relativistic ($\vec{\beta}_\perp \ll 1$) the equation of motion can be separated in a transverse and a longitudinal motion. We will then set $\gamma \approx \gamma_\parallel = \sqrt{1+u_\parallel^2}$.

3.7.1 Transverse Motion of Accelerated Electrons

The transverse equation of motion is

$$\frac{\partial}{\partial t}(\gamma_\parallel \vec{\beta}_\perp) = \vec{\nabla}_\perp \Phi_W(r,z,t)$$

In cylindrical coordinates this reads

$$\begin{aligned}&\gamma_\parallel \frac{\partial^2 r}{\partial t^2} + \frac{\partial \gamma_\parallel}{\partial t}\frac{\partial r}{\partial t} = \frac{\partial \Phi_W(r,z,t)}{\partial r} = \frac{\pi}{4} mc^2 a_0^2 \sin(\frac{\epsilon}{\beta_g}\xi)\frac{\partial g}{\partial r}(r,z) \\ &= -\pi \frac{1}{r_s(z)^2} a_0^2 \sin(\frac{\epsilon}{\beta_g}\xi) g^2(r,z) r \\ &\approx -\pi g_0(z)\frac{r_0^2}{r_s^4} a_0^2 \sin(\frac{\omega_p}{v_g}\xi) r = -\Omega_\perp^s \gamma_\parallel r \\ &\Rightarrow \frac{\partial^2 r}{\partial t^2} + 2\Gamma \frac{\partial r}{\partial t} + \Omega_\perp^s r = 0,\end{aligned}$$

where $\Omega_\perp s = \pi g_0^2(z)\frac{r_0^4}{r_s^6} a_0^2 \sin(\frac{\omega_p}{v_g}\xi)\frac{1}{\gamma_\parallel}$ and $\Gamma = \frac{\frac{\partial \gamma_\parallel}{\partial t}}{2\gamma_\parallel}$. Clearly $\Omega_\perp^s$ and Γ are due to the motion in longitudinal direction time dependent and therefore the solution to this equation is not just the damped harmonic oscillator. But when the two coefficients Γ and $\Omega_\perp^s$ are positive, this equation that the motion in the transverse direction is a damped oscillation with time dependent frequency $\sqrt{\Omega_\perp^s}$ and damping factor Γ, which is positive when the electron is accelerated longitudinally ($\frac{\partial \gamma_\parallel}{\partial t} > 0$). The problems of defocusing will occur when $\Omega_\perp^s$ is negative. Then the solution to harmonic oscillator becomes unbounded.

3.7.2 Longitudinal Motion of Accelerated Electrons

The longitudinal equation of motion is

$$\frac{\partial}{\partial t}\vec{u}_\parallel = \vec{\nabla}_\parallel \Phi_W(r,z,t),$$

which in cylindrical coordinates takes the form

$$\begin{aligned}\frac{\partial}{\partial t}\vec{u}_\parallel &= \frac{\partial \Phi_W(r,z,t)}{\partial z} = \frac{\pi}{2}\Phi_0(r)\frac{\epsilon}{\beta_g}\cos(\frac{\epsilon}{\beta_g}\xi) \\ &= \frac{\pi}{4}\frac{\epsilon}{\beta_g} a_0^2 g(r,z)\cos(\frac{\epsilon}{\beta_g}\xi).\end{aligned}$$

Here $\vec{u}_\parallel = \gamma_\parallel \vec{\beta}_\parallel$ is set. Using $\frac{\partial z}{\partial t} = \beta_\parallel = \frac{u_\parallel}{\sqrt{1+u_\parallel^2}}$ the Hamilton equations read

$$\frac{\partial z}{\partial t} = \frac{u_\parallel}{\sqrt{1+u_\parallel^2}} \tag{3.7.1}$$

$$\frac{\partial u_\parallel}{\partial t} = \frac{\pi}{4}\frac{\epsilon}{\beta_g} a_0^2 g^2(r,z)\cos(\frac{\epsilon}{\beta_g}\xi). \tag{3.7.2}$$

This set can be solved using numerical methods (see section 5).

3.8 Scaling Laws and Estimates

Regarding the experimental devices we are restricted by the laser with an pulse energy of E, the duration τ, the laser wavelength λ_L the width r_0 (see section 2). Whereas τ, r_0 and n_e are changeable variables. In this subsection we will give an overview and derivation of all the needed parameters. From now on we will only use CGS units. Also charges will therefore be measured in statC ($e = 4.8 \cdot 10^{-10}$ statC).

Plasma Density and Frequency The plasma wavelength λ_p and the length of the laser pulse have been set equal in equation 3.5.5. Using this definition of the plasma wavelength 3.2.5 the plasma density reads

$$n_0 = \frac{\pi m}{e^2 \tau^2},$$

which only depends on the parameters of the laser pulse. Accordingly the plasma frequency is given by

$$\omega_p = \frac{2\pi}{\tau}.$$

Normalized Vector Potential a_0 can be calculated from the formula 3.6, where U_L is now named E, the energy of the laser pulse. Note that g_0 has been set to one, since E is the initial energy.

$$a_0 = \sqrt{\frac{16E}{c\tau}}\frac{e}{mc^2 r_0 k_L}$$

Velocity of Pulse in Plasma and Length of Acceleration Region To estimate the necessary length of the plasma, the fact that electron will be highly relativistic most of the time of the acceleration is used. Therefore $v \approx c$, but the plasma wave travels with a speed

$$v_g = c\eta_r \approx c(1 - \frac{\omega_p^2}{2\omega_L^2})$$

and the length L_d the electron need to overtake half a wavelength of the plasma wave is then given by

$$L_d \approx \frac{\lambda_p^3}{\lambda_L^2}. \tag{3.8.1}$$

L_d is important since it gives an estimate after which length the maximal speed of the electron is reached and it starts decelerating again. Then it makes sence to set $L_d = L_{plasma}$.

Maximal Final Energy Knowing the length of the plasma and the maximal electrostatic force due to the plasma wave a rough estimate of the final energy is found by multiply both together.

$$E_{max} = mc^2 \frac{\pi^2}{2} \frac{\omega_L^2}{\omega_p^2}$$

Of course this value totally neglects depletion and refraction of the laser pulse and plasma wave.

Length of Defocusing If the existence of the plasma is totally neglected, i.e. set $\epsilon = 0$ in equation 3.5.4, the equation for Gaussian optics is recovered. There the characteristic length is given by the Rayleigh range

$$z_R = \frac{k_L r_0^2}{2}.$$

Since in the plasma we also have the so called relativistic self-focusing, which corresponds to the term in equation 3.5.4 proportional to ϵ^2 the Rayleigh range gives a lower bound on focus length. Nevertheless the effect of self-focusing is very small in the regime $a \ll 1$ since the formula is proportional to a^2. The effect can be seen, if we compare

$$4 \gg \epsilon^2 a_0^2 \overset{simulation}{\approx} 0.005,$$

where we have used that $n_0 = 1$ in dimensionless form and $g_0 = 1$ when the laser enters the plasma.

Length of Depletion An estimate for this length can be obtained if we calculate the length L_{dp} after which all of the energy of the laser has been used to generate the plasma wave. The argument is the same as in section 3.6, but only now we don't look at it infinitesimally and also switch of the effects of defocusing. The simplest approximation this yields

$$E_z^2 L_{dp} = E_L^2 L$$

. Plugging in the formula for the electric field of the laser and assuming $g_0 = 1$, $r_s = r_0$ the estimate reads

$$L_{dp} = L_d 2/a_0^2$$

Ionization of Gas Since in the experimental setup a gas jet (density n_0) is planed to be used, we have to show that our laser is strong enough to ionize the gas. This process is the plasma generation. For this to be the case the ponderomotive energy U_p of the laser needs to be much higher that the binding energy of a valence electron in the gas.

$$U_p \gg E_l$$

and U_p is given by

$$U_p = \frac{q^2}{2m_e \epsilon_0 c \omega_L^2} I$$

For our setup U_p is in the order of 80 keV.

3.9 Approximations and Assumptions

In this section the approximations made during the derivation of the linear model are discussed.

Small Dimensionless Vector Potential ($a^2 \ll 1$) and Fixed Shape This assumption is the most crucial to the calculation. It makes it possible to calculate every quantity as a truncated power series in a, which results in linear partial differential equations, that can be solved using an assumed shape of the laser pulse. Of course the form of the laser pulse will not be exactly the form we assumed, but the solution depends smoothly on the shape (linear PDEs). This means that if the actual shape of the laser pulse is only slightly different from the one we assumed the solution will also only change slightly.

Paraxial Approximation In order to describe the propagation of the laser pulse through the plasma the paraxial approximation was used,

$$\left|\frac{\partial a}{\partial \xi}\right| \ll \left|\frac{\partial a}{\partial z}\right|.$$

Both quantities can be estimated by setting $\frac{\partial a}{\partial z} \approx \frac{a}{\lambda_p}$ and $\frac{\partial a}{\partial t} \approx \frac{a}{\tau} = \frac{ac}{\lambda_p}$. Then the paraxial approximation is equal to

$$|c - v_g| \ll v_g,$$

which means that the wave has to travel almost the speed of light. This this is the case since $\epsilon \ll 1$.

Defocus Faster Than Deplete ($\left|\frac{\partial r_s}{\partial z}/r_s\right| \gg \left|\frac{\partial g_0}{\partial z}/g_0\right|$) This approximation claims that the relative change in the spot size is much stronger that the relative energy change of the wake governed by the creation of the plasma wake. Using the characteristic length for the two phenomena of depletion and defocusing the approximation can be found valid

$$\frac{z_R}{L_{dp}} = 2\pi r_0^2 \frac{\lambda_L}{\lambda_p^3} a_0^2 = 0.1 \ll 1.$$

4 Injection Methods

So far only the creation and propagation of the wake have been discussed. This chapter focuses on the injection, i.e. the method to trap electrons in the accelerating phase of the wave. In order to inject the electrons many different methods can be applied. They can be divided in two different categories, self-injection and controlled injection. The first experiments of plasma wake field acceleration were based on self-injection using relativistic wave breaking ([2],[16], [12] and many more). However this process only occurs in the highly nonlinear regime and is therefore not applicable to the setup presented. One problem of self-injection is the energy spread since electrons are constantly injected, which means that the electrons injected first have higher energies than the ones injected towards the end of the plasma channel. The main idea of controlled injection is to trap electrons only in a short section of the plasma, so the length of acceleration is for all trapped

electrons similar and therefore the energy spread is minimized. This work will focus on density down ramp injection and optical injection. There are also methods that make use of ionization and gas mixtures ([5], [11]). However they are more applicable to nonlinear plasma wakes and hence will not be presented here.

4.1 Theory of Injection for the 1D Linear Model

This chapter will follow the ideas of (reference). In the 1D model the contours of the Hamiltonian will describe the trajectories of the particles. The trajectories reveal the basic principles of injection. The relativistic Hamiltonian H of an electron in an electrostatic potential $\Phi(z - v_g t)$, which corresponds to the plasma wake, reads

$$H = mc^2(\gamma - 1) + e\Phi(z - v_g t).$$

Using the transformation

$$\Phi \to \frac{mc^2}{e}\Phi,\ H \to mc^2(H-1) \text{ and } \vec{p} \to mc\ \vec{u}$$

the Hamiltonian can be simplified to

$$H = (\gamma - 1) + \Phi(z - v_g t).$$

One has to be careful since the rescaling was not canonical and therefore the Hamilton equation change to

$$\frac{\partial z}{\partial t} = c\ \frac{\partial H}{\partial u_z}$$
$$\frac{\partial u_z}{\partial t} = -c\ \frac{\partial H}{\partial z}.$$

However scale transformations do not change the contours of the Hamiltonian, which is sufficient for this calculation. The next step is to move the Hamiltonian in a comoving coordinate frame by performing the canonical transformation $(z, u_z) \to (\xi, u_z)$, with a type 2 generating function $F_2(z, u_z) = u_z(z - v_g t)$. Note that the result

$$H' = H + \frac{1}{c}\frac{\partial F_2}{\partial t} = \sqrt{1 + u_\perp^2 + u_z^2} - \Phi(\xi) - \beta_g u_z$$

is independent of time. If the particle propagates through an electric field its momentum variable has to be modified to the canonical momentum $\vec{P} = \vec{p} - \frac{e}{c}\vec{A}$. In dimensionless coordinates this reads $\vec{U} = \vec{u} - \vec{a}$, where $\vec{a} = \frac{e\vec{A}}{mc^2}$. The trajectories of the particles can be calculated from the Hamiltonian

$$H = \sqrt{1 + (U_\perp + a)^2 + u_z^2} - \Phi(\xi) - \beta_g u_z \tag{4.1.1}$$

by extracting the contours in the (ξ, u_z) space. The equation of motion in the transverse direction

$$\frac{\partial U_\perp}{\partial t} = -\frac{\partial H}{\partial r_\perp} = 0 \Rightarrow u_\perp - a = \text{const}$$

reviles the quiver motion. Since the Hamiltonian is time independent its contours are the trajectories of the particles. Hamiltonian 4.1.1 can be formed into a quadratic equation in u_z which can be solved with

$$u_z = \gamma_g^2 \beta_g (H_0 + \Phi(\xi)) \pm \gamma_g \sqrt{\gamma_g^2 (H_0 + \Phi(\xi))^2 - \gamma_\perp}. \tag{4.1.2}$$

Note that each particle trajectory is now described by the transverse momentum $u_\perp$ hidden in $\gamma_\perp$ and the energy H_0.

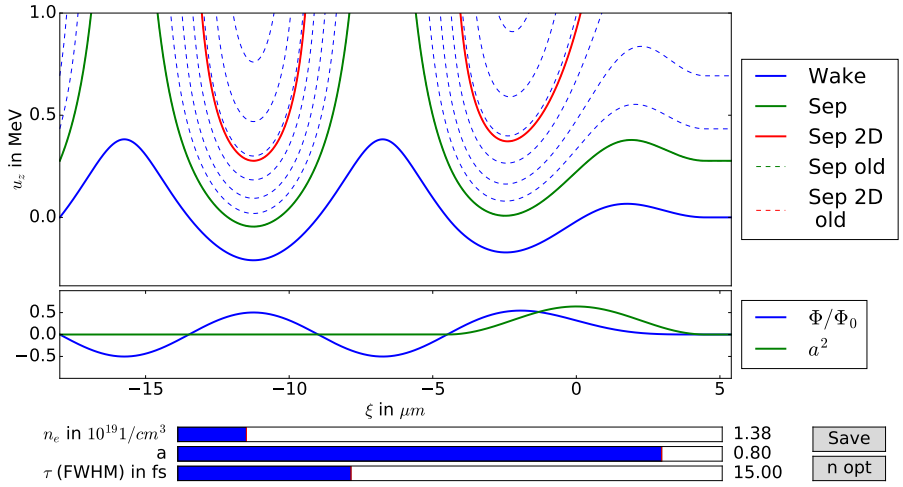

Figure 4: Plot of particle trajectories defined in equation 4.1.2. The parameters are set according to table 1.

Wake Electrons The initial conditions for plasma electrons are $\xi_i = +\inf$ and they are at rest $u_\perp(\xi_i) = u_z(\xi_i) = 0$, hence $H_0 = 1$.

1D Seperatrix The Separatrix is defined as the trajectory of the particles that has enough momentum to eventually overtake the laser pulse, which is propagates with v_g in the z direction. This means that on the Seperatrix there must be a point ξ_{min}, where the particle is traveling at the velocity of the wake β_g and it is neither accelerated nor decelerated. If a particle is only slightly faster that the seperatrix, it will be accelerated in the plasma wake over a large distance. In equations this means, that

$$\begin{aligned} \Phi(\xi_{min}) =& \Phi_{min}, \;\; E_z(\xi_{min}) = 0 \\ u_\perp(\xi_{min}) =& a(\xi_{min}), \;\; u_z(\xi_{min}) = u_g \\ \Rightarrow H_{sep} =& \frac{1}{\gamma_g} - \Phi_{min} \end{aligned}$$

2D Seperatrix The idea of the 2D Seperatrix is that we want the trapped particles to always stay in the transversely focusing phase of the wake.

$$H_{sep_{2D}} = \frac{1}{\gamma_g}$$

4.2 Density down-Ramp Injection

As shown in Section 3.2 we can write the plasma frequency as $\omega_p = \sqrt{4\pi n_e e^2/m}$, which is proportional to the electron density. Hence if the plasma density is increased, the plasma wavelength decreases. So by rapidely lowering the electron density it can be achieved

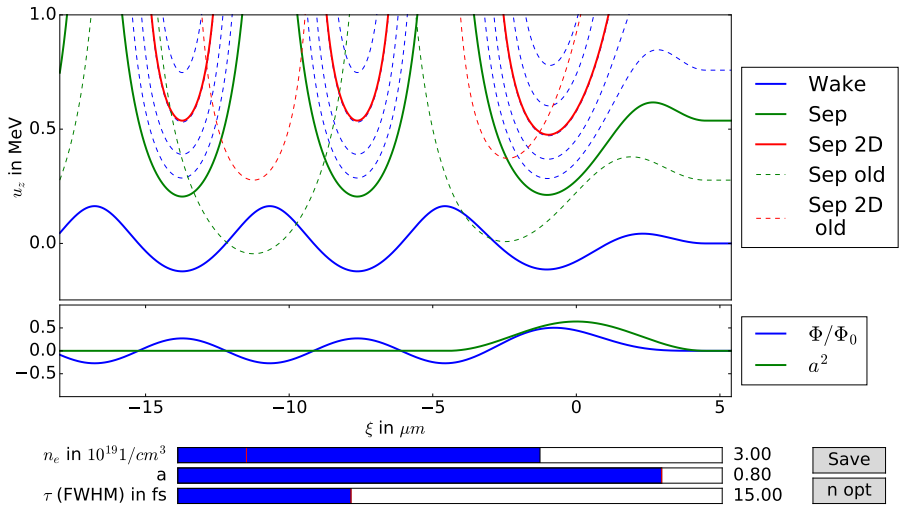

Figure 5: Plot of particle trajectories. The old configuration coincides with the setting found in the golden table 1 and plot 4. Since the solid blue line intersects the dashed green line we get injection into the plasma wake, which results with accelerated electrons

that some electrons have a configuration in phase space that lies above the seperatrix (dashed green line in plot 5) and they will therefore be accelerated to high energies. Such a high density in the beginning of the plasma can be achieved by introducing a shock wave in a supersonic gas jet. At the edge of a shock wave the density can change up to a factor of 3 withing a few micrometers ([15]). The shock wave can be generated by a knife. In section 5.2.1 the results of a numerical simulation of the density down ramp

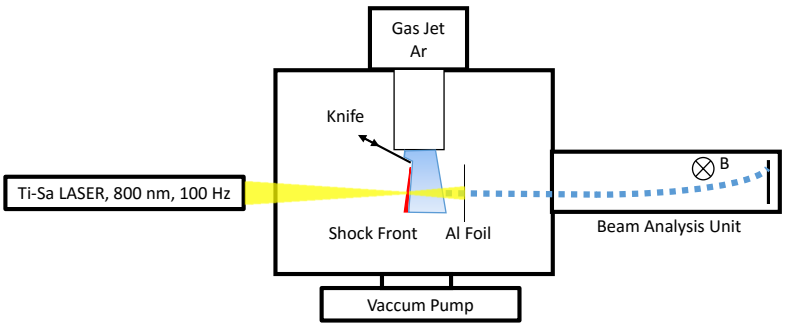

Figure 6: Experimental setup for Plasma Accelerator using Density Down Ramp Injection

injection process will be presented.

This technique is very simple to implement and gives the possibility to regulate the number of injected electrons by changing the position of the knife ([1]).

4.3 Optical Injection

The second major type on injection is optically. In contrast to the density down ramp injection you keep the density constant and inject electrons my modifying the laser. One can for example send in the plasma a second laser pulse, which is counterpointing to the diver laser to use the interference to accelerate electrons to high enough energies to be injected into the plasma wake ([9]). These methods require to have a second powerful pulsed laser or to split up the diver laser, which would result in final energy losses. Optical injection also requires an additional Optics, for example steerable mirrors, which is very expensive.

5 Numerical Simulations

From the simulations we expect to get an estimate on the charge, energy and divergence of the electron bunch. For the experiment it is also crucial to know how much radiation is produced. The energy can be estimated by solving the ODE for transverse and longitudinal motion for some electron with different initial conditions. At this point particle to particle coulomb interaction between the electrons will be neglected. A more elaborate, but also computationally more intensive method is to solve the problem of LWFA using the Particle-in-Cell method, which are discussed in Section 5.2. This method is more consisted, since it does not depend on any of the assumption done for the linear model. It rather solves the complete equations by discretizing space and time. It offers the possibility to study the effect of ionization of the gas, which is a major ingredient when working with a supersonic gas jet.

5.1 Single Particle Tracking

In this section the solution to the equations of motion of a single electron at initial condition $z_i = 5/2\lambda_p$ and $r_i = 0$ will discussed. The laser pulse is thought to be maximally focused to 8 µm at $z = 0$ mm. This can be most easily seen in figure 3. The solutions of g_0 and r_s give us an idea how strong the defocusing of the laser and its depletion effects the acceleration of electron. The solution of the equation of motion at perfect initial conditions will give us an upper bound to the expected energy γ of the electron. Let us start with solving g_0 and r_s. These variables are described by a system of two coupled ordinary differential equations 3.6.2 and 3.5.4. Whereas the one for g_0 is first order and r_s second order. As initial condition we have to choose

$$g_0\Big|_{z=0} = 1; \quad r_s\Big|_{z=0} = r_0; \quad \frac{\partial r_s}{\partial z}\Big|_{z=0} = 0.$$

These conditions express that the laser is maximally focused and has all its initial energy 40 mJ when the particles are injected (here $z = 0$). Note that $z = 0$ does not correspond the the beginning of the plasma, rather behind the density ramp, i.e. shock wave, described in sections 4.2 and 5.2.1. Figure 7 shows the numerical solution to that system of differential equations. This solution is then linearly interpolated in order to solve the motion of an electron in a depleting wave whose amplitude is described by equation 3.7.2, which depends on $g_0(z)$ and $r_s(z)$. In order to reach very high energies ($\beta\gamma > 1$) the elec-

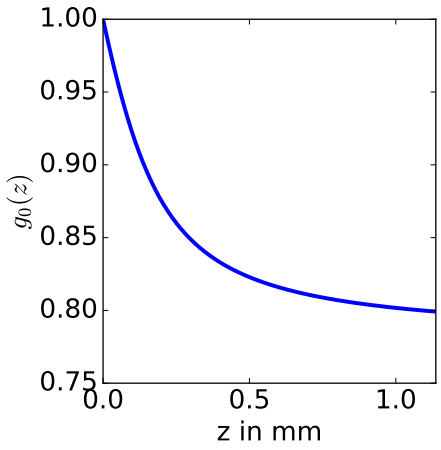

(a) $g_0(z)$ illustrates how much of the laser energy is converted into the energy of the electrostatic field of the plasma wave. We see that this effect dominates in the beginning, when the laser pulse enters the plasma.

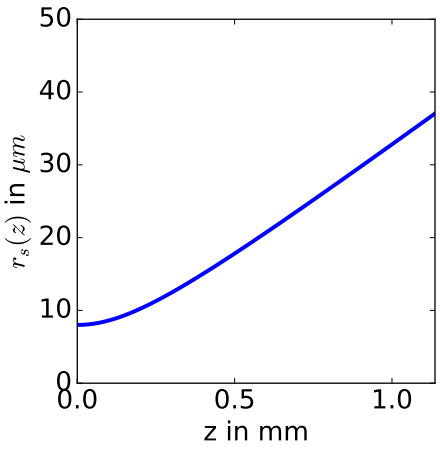

(b) The spot size $r_s(z)$ is a measure of the defocusing of the laser. Since we assumed the laser to be perfectly focused at $z = 0$ the effect of defocusing become more relevant to the end of the plasma.

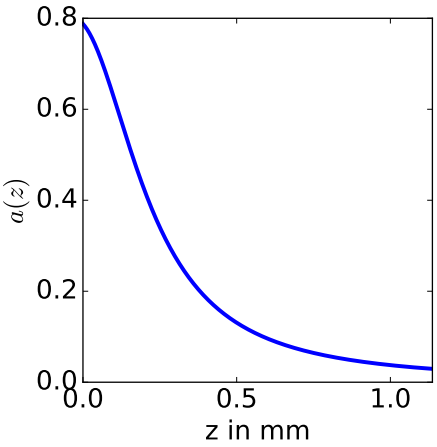

(c) $a(z)$ is related to the force that an electron feels in the plasma wave. We see that this force decays rapidly as the wave propagates through the plasma. After have of the length of the plasma channel the intensity, which is proportional to $a(z)^2$ has decreased to 1% of its initial value

Figure 7: Solution for the components of dimensionless vector potential a. The plots show how much the laser defocuses and deletes as a function of the width that it entered the plasma.

tron has to exceed the speed of the plasma wave before it enters the decelerating phase.

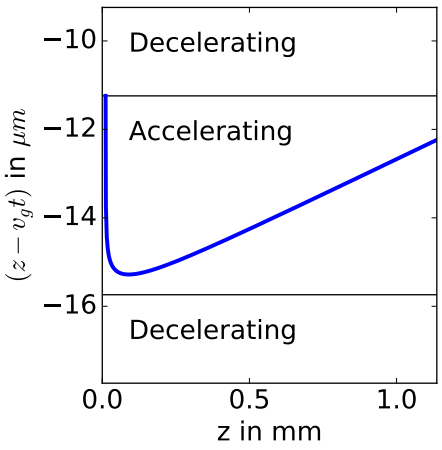

(a) The relative distance between the traveling wave and the accelerated particle viewed from the laboratory frame is shown in this plot. The accelerating phase corresponds to the phase in the wave where the particle feel a acceleration in the positive z direction. It is important to note that the electron never enters the decelerating phase and is therefore accelerated throughout the whole plasma.

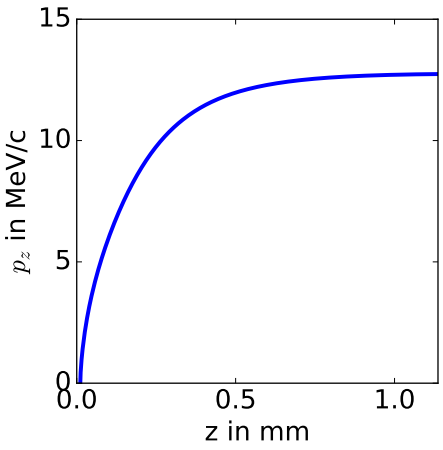

(b) in the high relativistic limit $\beta\gamma \approx \gamma$. The kinetic energy of the particle is given by $mc^2(\gamma - 1)$. The plot therefore gives an direct measure of the energy of the energy of the accelerated electron. We see that only in the first half of the plasma channel the electron is accelerated significantly and reaches a final kinetic energy of 12 MeV.

Figure 8: These plots are related to the solution of the motion of a single particle in a plasma wave that is generated by a defocusing and depleting laser pulse.

This overtaking process happens on a longer length scale than the plasma wavelength, therefore higher energies are reached ($E = Fs$). A limitation to the acceleration length is the dephasing, which means the electron rides the wake so far that in enters the decelerating phase. This is similar to surfing out a wave to the front. Formula 3.8.1 gives a good estimate to the distance when this happens and also the length of the plasma channel L_{plasma} is set to that estimate

$$L_{plasma} = \frac{\lambda_p^3}{\lambda_L^2}.$$

5.2 Particle-in-Cell Simulation

The basic idea of the Particles-in-Cell (PIC) Method is to introduce a grid over the simulation domain and macroparticles with the same mass to charge ratio as an electron. The grid will be used to solve Maxwell's equations. The particles will be pushed using a Leap Frog method. The forces on macroparticles are calculated with the Lorenz Force Equation. However the electric and magnetic fields have to be interpolated from the grid points to the position of the particles. There are many different approaches to optimize the performance and numerical stability of such a code. The presented simulations

have been performed using the code WARP in the quasi-cylindric coordinates that are described in [10]. For more information look into the input file `warp_script.py` in the project folder and the documentation of `warp-initialization-tools` by Remi Lehe (`https://bitbucket.org/remilehe/warp-initialization-tools`).

5.2.1 Quality of Injection and Acceleration

In order to simulate the Density Down Ramp Injection process it is important to fix a density distribution. At this point the density distribution has not been measured yet, so an educated guess has been used. In order to estimate the density distribution of shock fronts in supersonic gas jets several papers have been consulted ([15], [1], [13]).

Using this information and manually optimizing for the parameters the distribution found in figure 9 appeared most reasonable. Of course this is just a coarse approximation and in the future a simulations and analysis with the real measured density distribution will have to be performed.

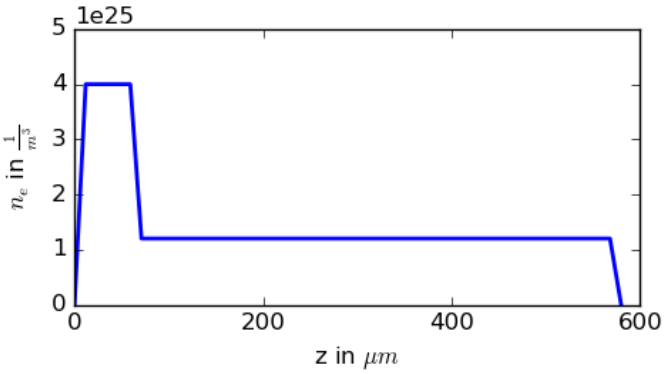

Figure 9: Electron density for PIC simulation. After looking at the ionization of argon it can be seen that in order to get the ion density n_e has to be divided by 8 (Ar^{8+}).

The laser was set to be maximally focused at the down ramp ($\approx$ 80 µm) to the parameters listed in the golden table 1. The results in figure 10 indicate that the injection and acceleration behave very similar to the linear model of injection presented in section 4, which predicted that some injection would occur. The energy prediction of the linear model of about 10 MeV/c was off by a factor of 2 most probably because the depletion (Section 3.6) was overestimated.

The plots of figure 11 show two bunches moving with a separation of 10 µm, a total charge of 4 pC, mean momentum of 16 MeV/c and a divergence of 40 mrad. The transverse emittance of the bunches is of the order of 1 mm mrad, which is an order of magnitude ($\approx$ factor of 20) higher that what can be achieved by conventional accelerators, like they are used for Free Electron Lasers. The major problem of this accelerator is the energy spread. With $\frac{\Delta E}{E} \approx 0.7$ we cannot speak about a real mono-energetic beam anymore. This problem is due to that fact, that the injected electron spend long time in the defocusing/accelerating phase of the plasma wake. When the electrons get pushed out to larger radii they feel different accelerating forces. When the laser would have more

energy all injected electrons would stay in the focusing/accelerating phase and smaller energy spread could be reached.

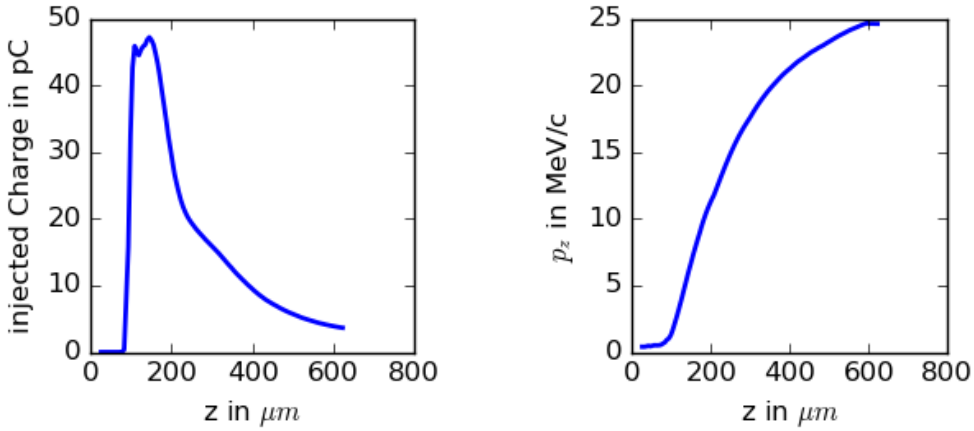

(a) Number of particles with $\beta\gamma > 1$. This corresponds to the accelerated electrons since in the linear regime all wave electrons have $\beta\gamma < 1$.

(b) Maximal momentum in propagation direction z. This does not correspondent to the mean energy of the bunch.

Figure 10: The pictures clearly show the density injection process. At about 80 µm the momentum of the particles suddenly starts increasing. This is the point where the Density Down Ramp was placed.

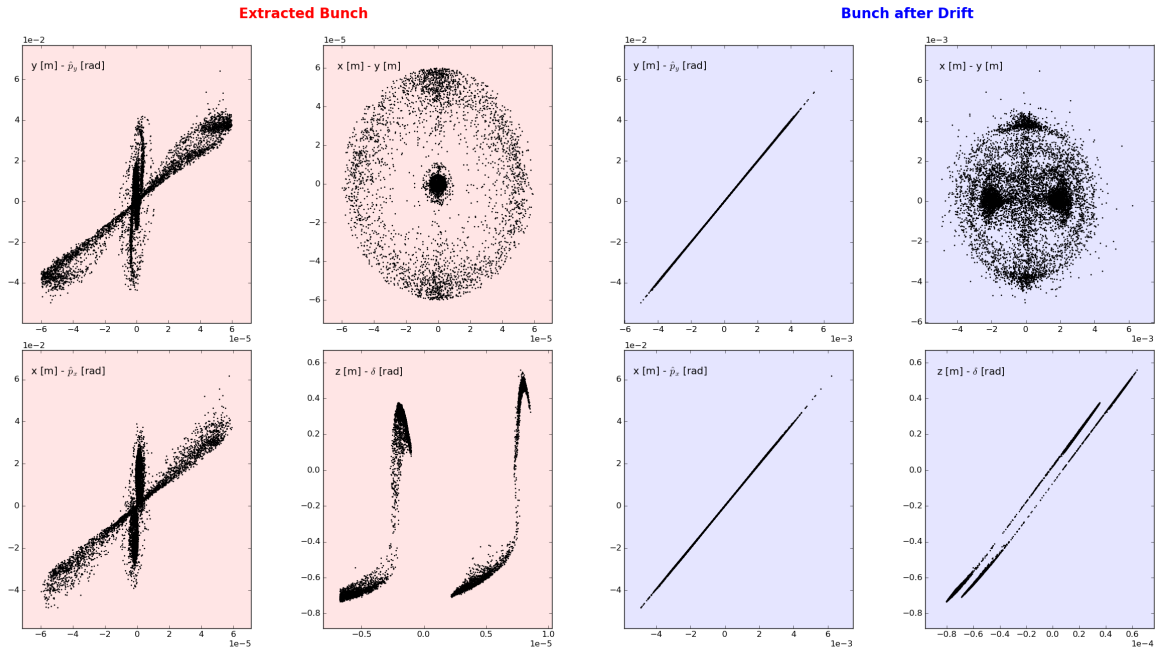

Figure 11: This plots show the properties of the extracted beam. Note that the right for plots show the configuration of phase space after a 10 cm drift. The particles have been pushed using the linear approximation of beam optics, which is in this case valid since $\delta, u_x, u_y \ll 1$. Note that all coordinates are dimensionless. δ is the dimensionless energy divination.

5.2.2 Radiation safety

In order to perform experiments with accelerated electrons it is important to estimate the charge and energy of the electrons. For this reason during the simulation all the particles that left the simulation domain with momentum above 1 MeV/c have been collected. From this an angular and energy distribution is calculated. The total charge of not co-linear to the laser accelerated particles is of the order of 35 pC. A mean momentum of 2.2 MeV/c has been reached.

Double counting of the particles could be avoided by taking into account the momentum of the particles. Particles that are in a shell of a cylinder of radius greater that the laser focus, here 15 µm. The thickness of the shell varies depending on the momentum of the particles, i.e. $v_p \tau_{sim}$, where v_p is the velocity of the particles perpendicular to the cylinder and τ_{sim} is the time step of the simulation.

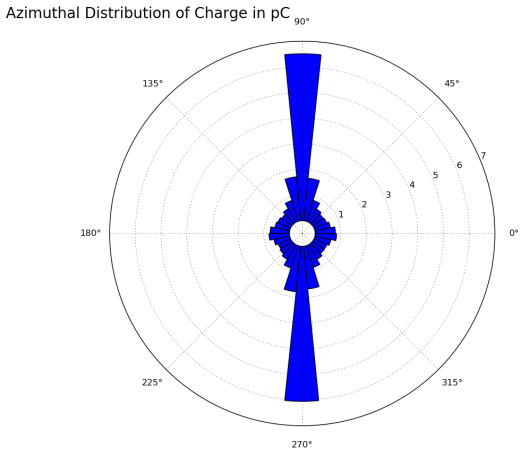

(a) The transverse angular distribution of produced strongly divergent particles (not in the final bunch).

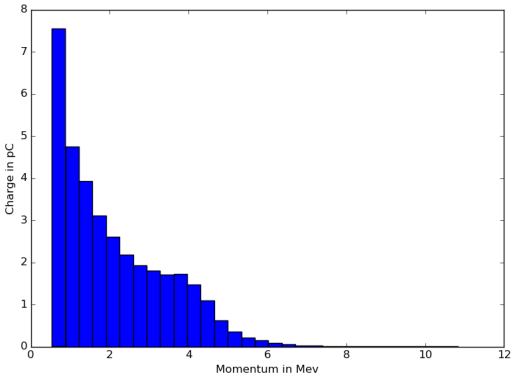

(b) The energy distribution of produced strongly divergent particles (not in the final bunch).

Figure 12: These plots give an estimate of the accelerated charges in the accelerator that are not confined in the beam pipe.

6 Golden Table for Experimental Setup

For the simulation we set some parameters which are important to get the results shown in section 5.

Parameter	**Value**	**Parameter**	**Value**
E	40 mJ	n_e	$1.4 \times 10^{25}\,/\mathrm{m}^3$
ω_p	$2.1 \times 10^{14}\,\mathrm{s}^{-1}$	a_0	0.8
τ (FWHM)	15 fs	L_{plasma}	0.6 mm
k_L	800 nm	z_R	0.25 mm
Q_{bunch}	4 pC	acceleration gradient	$32\,\mathrm{GeV\,m}^{-1}$
r_0	8 µm		

Table 1: Parameters of for Simulations and Experiment

7 Conclusion and Outlook

In order to really implement a wake field accelerator many more experimental problems, like characterizing the density profile of the gasjet, setting up the beam diagnostics or

installing the laser optics have to be solved. However this theoretical work demonstrates that implementing a wake field accelerator at PSI is possible.

The energy, size and repetition rate of 100 Hz suggest using this source for Ultra Fast Electron Diffraction (UFED) experiments. Usually UFED setups are very cost intensive and need large space. With our work we want to demonstrate that such devices can be build using high power femtosecond lasers, which are available in many laboratories, especially also at the SwissFEL here at PSI.

Notation and Symbols

ϵ	$\frac{\omega_p}{\omega_L}$ dimensionless plasma frequency
ω_L	laser frequency
ω_p	plasma frequency
Φ	electrostatic potential
τ	duration of laser pulse
$\vec{a}(\vec{r},t)$	dimensionless vector potential
$\vec{Q}_\parallel$	longitudinal component of vectorial Quantity $\vec{Q}$
$\vec{Q}_\perp$	transverse component of vectorial Quantity $\vec{Q}$
ξ	co-moving coordinate of laser pulse $\xi = z - v_g t$
a_0	initial peak magnitude of dimensionless laser pulse vector potential
$f(\xi)$	longitudinal shape of laser pulse
$g(r,z)$	transverse shape of laser pulse including defocusing and depletion
L_{dp}	characteristic length of depletion of the laser pulse
L_{plasma}	z extension of plasma
n	electron density
n^0	background ion density
Q_n	term in expansion of Quantity Q proportional to a^n
r_0	focal radius
u	dimensionless momentum
v_g	group velocity of laser pulse
z_R	Raleigh length, characteristic length of defocusing of the laser pulse

References

[1] A. Buck, J. Wenz, J. Xu, K. Khrennikov, K. Schmid, M. Heigoldt, J. M. Mikhailova, M. Geissler, B. Shen, F. Krausz, S. Karsch, and L. Veisz. Shock-front injector for high-quality laser-plasma acceleration. *Phys. Rev. Lett.*, 110:185006, May 2013.

[2] S.V. Bulanov, L.M. Kovrizhnykh, and A.S. Sakharov. Regular mechanisms of electron and ion acceleration in the interaction of strong electromagnetic waves with a plasma. *Physics Reports*, 186(1):1 – 51, 1990.

[3] R. N. Chen, X. L.; Sudan. Two-dimensional self-focusing of short intense laser pulse in underdense plasma. *Physics of Fluids B: Plasma Physics*, 5:1336, Apr 1993.

[4] C. Chiu, S. Cheshkov, and T. Tajima. High energy laser-wakefield collider with synchronous acceleration. *Phys. Rev. ST Accel. Beams*, 3:101301, Oct 2000.

[5] F. G. Desforges, B. S. Paradkar, M. Hansson, J. Ju, L. Senje, T. L. Audet, A. Persson, S. Dobosz-Dufrenoy, O. Lundh, G. Maynard, P. Monot, J.-L. Vay, C.-G. Wahlstrom, and B. Cros. Dynamics of ionization-induced electron injection in the high density regime of laser wakefield acceleration. *Physics of Plasmas*, 21(12), 2014.

[6] Carl Eckart. Variation principles of hydrodynamics. *Physics of Fluids*, 3(3):421–427, 1960.

[7] E. Esarey, C. B. Schroeder, and W. P. Leemans. Physics of laser-driven plasma-based electron accelerators. *Rev. Mod. Phys.*, 81:1229–1285, Aug 2009.

[8] E. Esarey, P. Sprangle, J. Krall, and A. Ting. Self-focusing and guiding of short laser pulses in ionizing gases and plasmas. *Quantum Electronics, IEEE Journal of*, 33(11):1879–1914, November 1997.

[9] J. Faure, C. Rechatin, A. Norlin, A. Lifschitz, Y. Glinec, and V. Malka. Controlled injection and acceleration of electrons in plasma wakefields by colliding laser pulses. *Nature*, 444(7120):737–739, Dec 2006.

[10] A.F. Lifschitz, X. Davoine, E. Lefebvre, J. Faure, C. Rechatin, and V. Malka. Particle-in-cell modeling of laser-plasma interaction using fourier decomposition. *Journal of Computational Physics*, 228(5):1803 – 1814, 2009.

[11] A. Pak, K. A. Marsh, S. F. Martins, W. Lu, W. B. Mori, and C. Joshi. Injection and trapping of tunnel-ionized electrons into laser-produced wakes. *Phys. Rev. Lett.*, 104:025003, Jan 2010.

[12] A. Pukhov and J. Meyer-ter Vehn. Laser wake field acceleration: the highly non-linear broken-wave regime. *Applied Physics B*, 74(4):355–361, 2002.

[13] Karl Schmid. Supersonic micro-jets and their application to few-cycle laser-driven electron acceleration. Juli 2009.

[14] R.L. Selinger and G.B. Whitham. *Proc. R. Soc. London*, Ser. A:305, 1968.

[15] Chunmei Wang, Ji Li, Jun Sun, and Xisheng Luo. Shock-wave-based density down ramp for electron injection. *Phys. Rev. ST Accel. Beams*, 15:020401, Feb 2012.

[16] G.B. Whitham. *Linear and Nonlinear Waves*. 1974.